ORNL/CP-99005
CONF-980657--

EFFECTS OF INTERACTIVE PARTICLES ON STEEL WELDABILITY

C. van der Eijk[1], Ø. Grong[1], S.S. Babu[2], and S.A. David[2]
[1] Norwegian University of Science and Technology, Department of Metallurgy, N-7034 Trondheim, Norway.
[2] Metals and Ceramics Division Oak Ridge National Laboratory, TN 37831-6095, USA.

Abstract

The concept of intragranular ferrite nucleation by specific inclusions is well known from steel weld metals. In this paper it is shown that the idea can be transferred to steel metallurgy. Control of the inclusion composition and thus the nucleation potency with respect to ferrite can readily be achieved by the choice of an appropriate deoxidation procedure. Thermodynamic (Thermo-Calc) calculations in addition to X-ray mappings and microprobe analysis are employed to understand and predict the inclusion formation in the steels. Three different steels, two of them Ti-deoxidised, and one Al-Ca-deoxidised, have been subjected to weld thermal simulation at different peak temperatures and cooling programmes followed by Charpy-V notch testing at -40°C to reveal differences in the HAZ toughness. The results from these tests show that the titanium deoxidized steels exhibit excellent toughness in the grain coarsened HAZ after high heat input weld simulation because of a refinement of the microstructure. This observation is in contrast to the more traditional behaviour of the conventional Al-Ca deoxidized steels, which show no evidence of intragranular ferrite formation.

Introduction

The major impetus for developments in low-carbon microalloyed steels have been provided by the need for improved weldability. In particular, steels that can be welded with high heat input are usually preferred since they represent a potential for reduced fabrication costs. However, the current trend towards the use of stronger steels and heavier sections has lead to an increased emphasis on the HAZ toughness which tends to deteriorate at high heat inputs[1]. Due to this, a new class of low-carbon microalloyed steels, which utilises the concept of intragranular nucleation of acicular ferrite as a means to improve the HAZ toughness in the as-welded condition, has emerged over the last years [2-4]. These steels are not aluminium-killed, but are instead deoxidized with titanium to produce a relatively coarse distribution of complex Ti-oxide inclusions within the base metal. During high heat input welding (> 5 kJ mm^{-1}), the oxides will not retard austenite grain growth, as compared to TiN, but instead act as favourable nucleation sites for acicular ferrite within the interior of the austenite grains [5], and thereby refine the effective grain size. This concept is illustrated in Fig. 1.

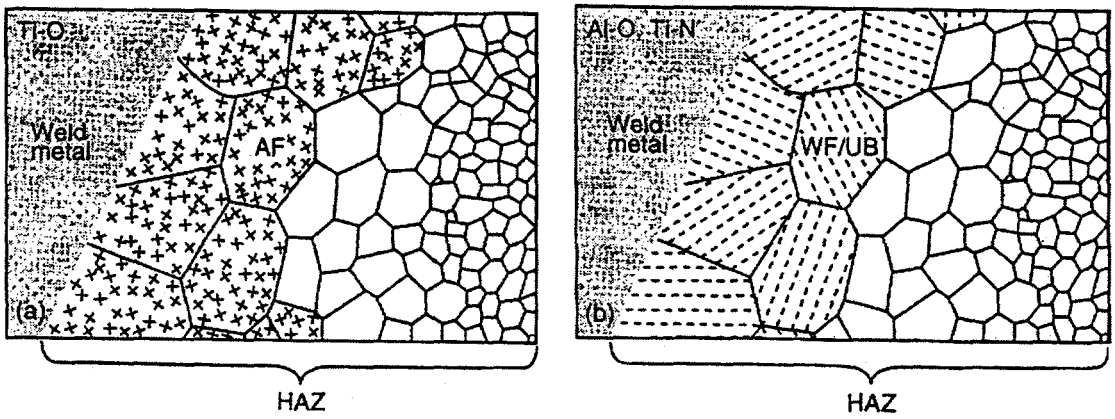

Figure 1. Schematic illustration of the HAZ transformation behavior during high heat input welding; (1) Ti-oxide containing steel, (b) conventional Al-Ti microalloyed steel[5].

DISCLAIMER

However, since the inclusion number density is quite low ($<10^4$ particles per mm^3), the microstructure is significantly coarser than that normally observed in steel weld deposits [6-10]. Nevertheless, their presence contributes to suppress the formation of Widmanstätten ferrite and upper bainite within the grain coarsened HAZ, which is a common problem with the traditional microalloyed steels [1,5].

Experimental

Three continuously cast slabs (thickness 288 mm), in the following designated steels A, B and C, were received from Dillinger Hüttenwerke. The steels A and B were deoxidized using Ti, while C is a reference steel which was deoxidized using Al-Ca. The chemical compositions of the experimental steels are listed in Table 1.

The steels are TMCP rolled to a plate thickness of about 80 mm. Specimens with dimensions 11x11x100 mm were cut from the plates and subjected to weld thermal simulation using a Smitweld thermal simulator (model 1405). The simulated thermal cycles represent varying cooling times from 800°C and 500°C ($\Delta t_{8/5}$) i.e. 5, 10, 20, 40 sec. The corresponding peak temperatures T_p were 1050°C, 1150°C, 1250°C and 1350°C. After weld thermal simulation, the samples were machined into standard Charpy V notch (CVN) specimens and subjected to impact testing at a temperature of -40°C. The simulated HAZ microstructures were examined in a Leica, Reichert MeF3A optical microscope. Examinations of the fracture surface of some broken CVN specimens were carried out with a Jeol 840 scanning electron microscope.

The EDS analyses of the inclusions present in the as-cast materials were done with the same microscope at three different slab positions. A total of 50 inclusions was examined in each case. The acceleration voltage was 20 kV. The results were normalized to eliminate the effect of Fe signals from the steel matrix.

Moreover, the size distribution of oxides larger than 1 μm was measured in samples extracted from the center, the quarter thickness and the surface of the slab. The size distributions are obtained from micrographs equivalent to an area of 4 mm^2 by image analyses. The microprobe investigation was done using a Jeol JXA-8900 M microscope equipped with both an EDS and a WDS unit. Complete X-ray mapping was done on a representative inclusion in steel A in the as-rolled condition.

Finally, Thermo-Calc[6] calculations were performed to predict the oxide composition and unravel the sequence of precipitation reactions taking place both before, during and after solidification due to interactions between oxygen, sulphur and nitrogen and different alloying elements present in the steels. These calculations were performed assuming full equilibrium at all times, except in the solid state where equilibrium is restricted to a small volume of metal enclosing the inclusions.

Results & Discussion

A. CVN testing

Since all three steels revealed good toughness after weld simulation within the peak temperature range from 1050 to 1250°C, these results are omitted in the presentation. However, when the peak temperature was increased to 1350°C, the response was different, as shown by the CVN data in Fig. 2. These values are the average of 6 different tests. The individual results showed large scatter.

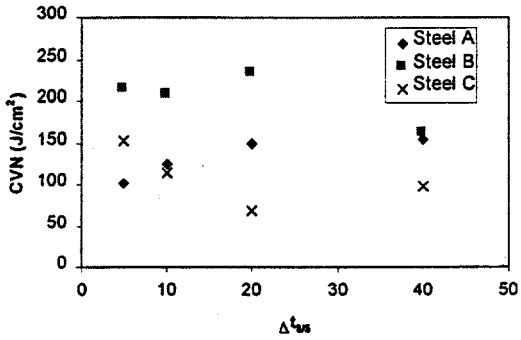

Figure 2. Results from CVN testing of the three steels at –40°C, average of 6 different tests (simulated specimens, T_p=1350°C).

Table 1. Chemical compositions of experimental steels (wt%).

Steel	C	Si	Mn	P	S	Al	N	O	Ni	Nb	Ti	Ca	Cu
A	0.078	0.08	1.55	0.011	0.005	0.002	0.0034	0.0042	0.37	0.013	0.009	0.0009	0.23
B	0.059	0.09	1.40	0.008	0.004	0.002	0.0020	0.0022	0.24	0.018	0.023	0.0005	0.08
C	0.072	0.11	1.50	0.012	0.003	0.037	0.0044	0.0022	0.26	0.017	0.010	0.0027	0.13

In spite of the observed scatter in the results, the Ti-deoxidized steels (steels A and B) reveal a better toughness after high heat input weld simulation compared with the traditional Al-Ca deoxidized steel (steel C). In order to explain the scatter in the results, especially between parallels, SEM fracture analyses were employed. These analyses show that brittle fracture in steel B is initiated at inclusions. Especially large inclusions (>10 μm) and pairs of inclusions close to each other seem to be detrimental to toughness. An example of this is shown in Fig. 3. It is obvious that the fracture is initiated from one of the inclusions. The white spots within the inclusions are caused by the EDS analysis. Both the inclusions have the expected composition. In this specific specimen, the CVN-value was 14 J/cm^2 while the average value was 233 J/cm^2. In contrast, the low toughness of some of the other specimens from steels A and C could not be traced back to inclusions and may thus originate from microstructural heterogeneity. Note that the reduced HAZ toughness of steel A at low heat input weld simulation is due to the higher carbon equivalent of this steel compared with the steels B and C, which leads to formation of upper bainite and M-A phases during the γ to α transformation.

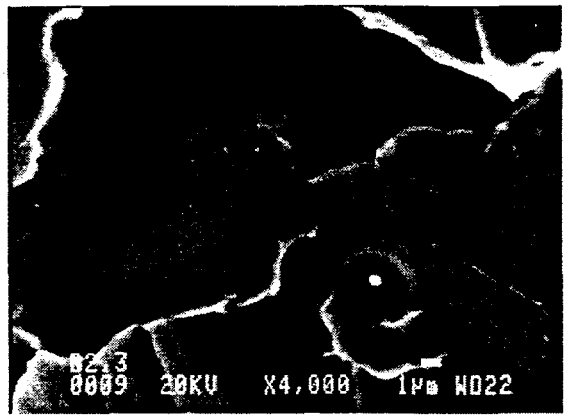

Figure 3. SEM micrograph showing evidence of brittle fracture initiation at an inclusion in steel B (simulated specimen, T_p=1350°C, $\Delta t_{8/5}$=20 s).

B. Ferrite nucleation at inclusions

The toughness improvement observed in the Ti-deoxidized steels is thought to be related to a change in the HAZ transformation behavior due to presence of more favourable inclusions. As shown in Fig. 4, both steels A and B showed evidence of intragranular nucleation of ferrite at inclusions in the grain coarsened HAZ. In contrast, no intragranular nucleation events could be observed in steel C, which confirms that the inclusion chemistry, as affected by the applied deoxidation practice, plays an important role in the microstructure development. Over the years different mechanisms have been proposed to explain the intragranular nucleation phenomenon, including [7-12]:

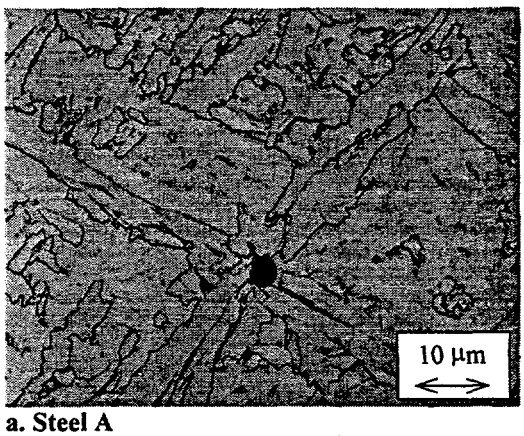

a. Steel A

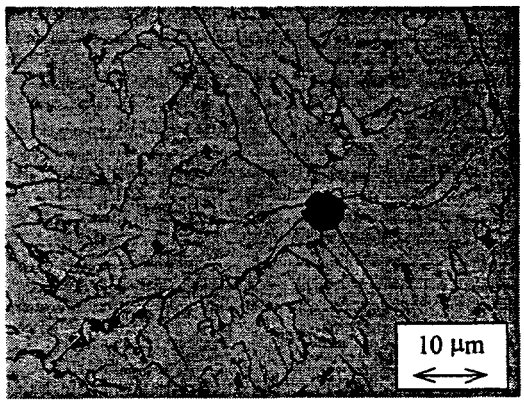

b. Steel B

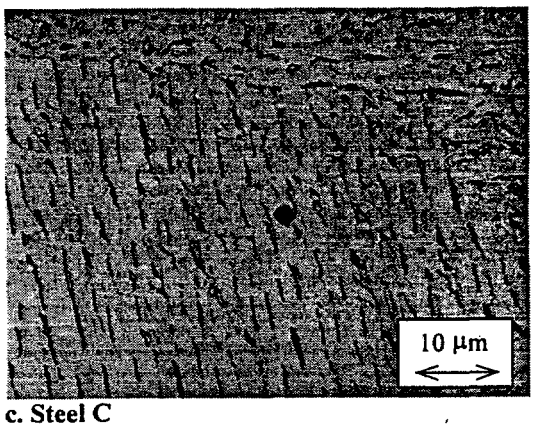

c. Steel C

Figure 4. Optical micrograph showing evidence of intragranular nucleation of ferrite at inclusions in steels A and B, but not in steel C. Simulated specimens, T_p=1350°C, $\Delta t_{8/5}$=40 s.

(i) Nucleation resulting from a small lattice disregistry between the inclusions and the ferrite.
(ii) Nucleation in the vicinity of inclusions resulting from favourable strain or dislocation arrays due to differences in thermal contraction between the particles and the matrix.
(iii) Nucleation in the vicinity of inclusions caused by local compositional inhomogeneity in the steel matrix.

Because of the complexity of the inclusions, and the experimental difficulties involved in performing controlled in situ measurements, it cannot be stated with certainty which of these three mechanisms that is operating during the intragranular ferrite formation.

In order to explain the observed change in the HAZ transformation behavior, the following discussion will be directed towards the mechanisms of inclusion formation during steel deoxidation and solidification.

C. Inclusion characteristics

The average size (three dimensional particle diameter), volume fraction and composition of the oxi-sulphide inclusions are shown in Table 2. Steel A contains MnS, few SiO_2 and complex oxi-sulphide inclusions. Pure MnS inclusions are observed up to a size of 6 μm, while the SiO_2 inclusions are about 1 μm. Steel B contains submicroscopic particles of MnS and complex oxi-sulphide inclusions. No SiO_2 inclusions are observed in steel B. In steel C, the inclusions are Al-Ca oxides as commonly observed in such steels. The Mg found in the inclusions stems probably from the lining of the treatment ladle. Small TiN precipitates are also present in steels B and C.

Fig. 5 shows the appearance of the different phases in an inclusion localized in steel A. It follows that the oxide core contains Al, Ti and Mn. The Al-oxide does not mix with the Ti-Mn-oxide. Mn and S are present on the surface of the inclusion, presumably in the form of MnS. In addition, the examination carried out in the optical microscope showed that TiN is present on the surface of the inclusion as gold-coloured cubes. These findings are consistent with those reported by others [4, 13-15].

A better understanding of the inclusion formation is possible if the thermodynamic stability of the different phases is considered. The sequence of inclusion formation, according to Thermo-Calc, is shown in Fig. 6. Before and during solidification the oxide core forms. If Ti deoxidation is employed, the amount of stable oxides will increase considerably during solidification. This is in sharp contrast to steel C, which is Al-Ca deoxidised, where the oxide formation is completed in the liquid state. Therefore, no increase in the amount of stable oxides is expected during solidification. In the final stage of solidification, MnS will start to precipitate both in the interdendritic region and on the surface of the oxides. The formation of TiN on the inclusions will take place at even lower temperatures. Since most of the Ti is consumed in oxide formation, the amount of free Ti available for TiN-formation is limited.

However, the TiN formation on the surface of the oxides is possible if Ti is extracted form the core. Thermo-Calc predictions carried out on a closed system show that replacement of Ti by Mn is thermodynamically favourable and will lead to formation of TiN on the surface of the inclusions. Thus, the TiN formation can be represented by the following exchange reaction:

$$\underline{N} + \underline{Mn} + Ti_2O_3 \rightarrow TiN + MnOTiO_2$$

The predicted $MnOTiO_2$ formation is in good agreement with the X-ray data in Fig. 5, which show that Mn concentrates in the same area as N and Ti. The calculations done with Thermo-Calc state that, at the end of solidification, the oxides in steel A should consist of mainly Ti with some Al and Ca, while in steel B the core should be pure Ti_2O_3. By correcting the data in Table 2 for the presence of MnS, the composition of the oxide core can be determined. It follows that the experimental results are in fair agreement with the Thermo-Calc predictions.

Table 2: Inclusion characteristics (as-cast condition), compositions in wt%.

	A	B	C
average size, (μm)	3.3	2.7	3.3
incl. volume fraction	5.8×10^{-4}	4.1×10^{-4}	6.0×10^{-4}
Ti	29.9	50.5	1.6
Al	18.3	3.9	23.3
Mn	35.0	31.0	12.4
S	10.1	11.0	23.4
Ca	4.0	2.1	27.8
Mg	1.6	1.4	11.5
Si	1.0	0.2	0.1

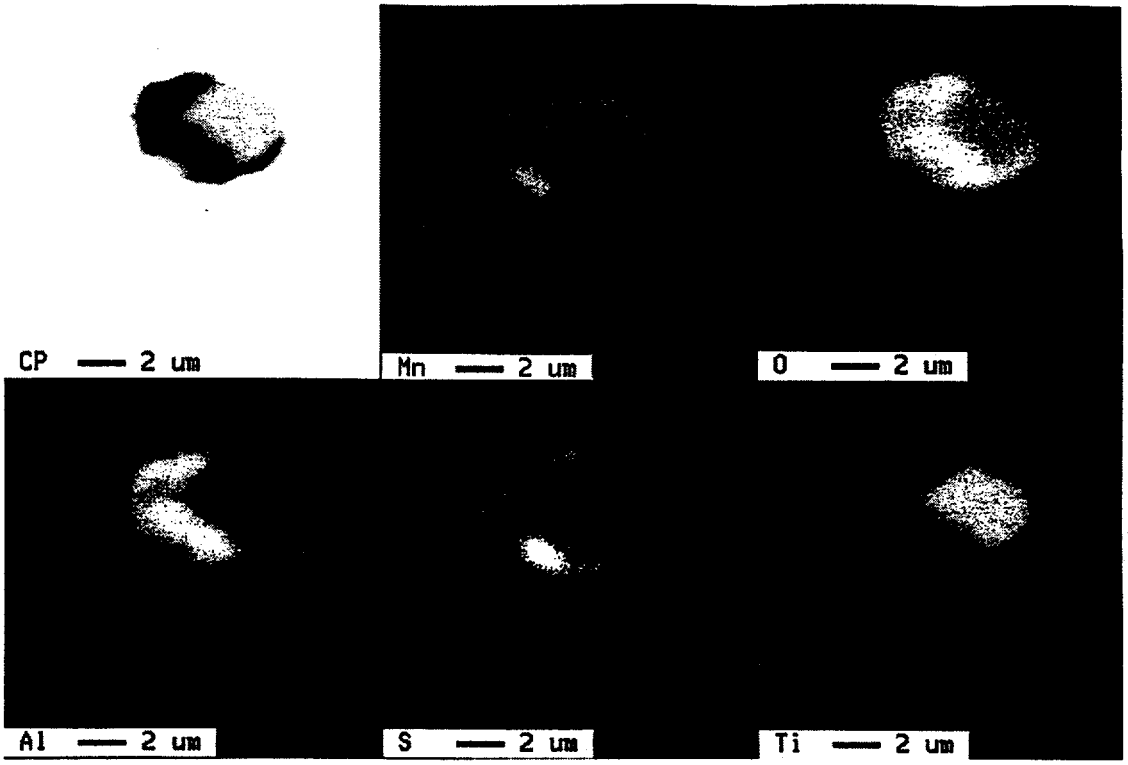

Figure 5. X-ray mapping of an inclusion in steel A (as-rolled condition).

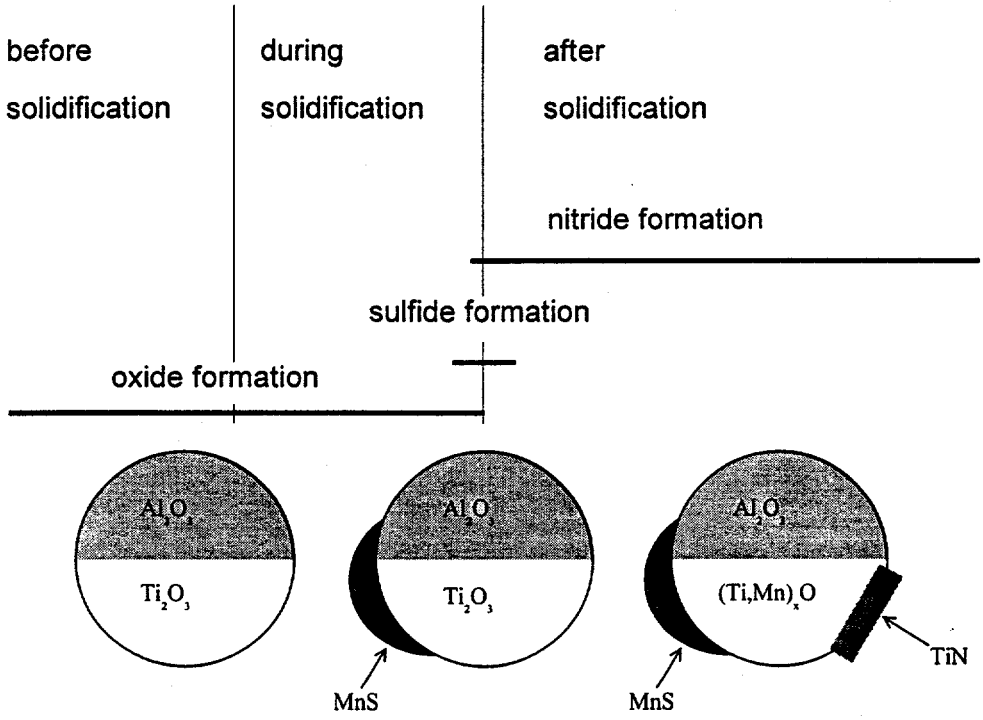

Figure 6. Schematic representation of the sequence of inclusion formation in Ti-deoxidised steels. The figure is drawn on the basis of outputs from Thermo-Calc.

At present, it cannot be stated with certainty which mechanism that is operative in the Ti-deoxidized steels and causes intragranular nucleation of ferrite at inclusions within the grain coarsened HAZ during welding. It is clear, however, that the final inclusion composition is the result of reactions occurring both in the treatment ladle, during solidification and in the solid state, and that the observed catalyst effect is related to the presence of specific constituent phases at the surface of the inclusions. Attempts are currently being made to explore the underlying nucleation mechanisms more in detail, using advanced electron microscopy and in-situ texture analyses (EBSP). These results will be reported in forthcoming publications.

Conclusions

1. In general, the Ti-deoxidized steels A and B show a better toughness after high heat input weld simulation than the conventional Al-Ca deoxidised steel C. This is due to the presence of the Ti-oxide inclusions, which interact with the iron matrix during the weld thermal cycle and stimulate intragranular nucleation of ferrite.

2. Thermo-Calc predicts that the inclusions form in the sequence: oxide, sulphides, nitrides. This is consistent with experimental observations, which show that the inclusions consist of an oxide core with sulphides and nitrides present at the surface.

3. The indications are that the ferrite nucleation potency of the inclusions is related to the presence of specific constituent phases at the surface, which may form during solidification and /or in the solid state. Thermo-Calc predictions carried out on a closed system show that Mn from the adjacent steel matrix can replace Ti in the oxide core, with consequent formation of TiN and $MnOTiO_2$.

Acknowledgement

The research effort by S. S. Babu and S. A. David was sponsored by the Division of Materials Sciences, U.S. Department of Energy, under contract DE-AC05-96OR22464 with Lockheed Martin Energy Research Corporation.

References

1. Ø. Grong and O. M. Akselsen, Metal construction, 1986,18, 557-562.
2. F. J. Barbaro, P. Krauklis and K. E. Easterling, Mater. Sci. Technol., 1989, **5**, 1057-1068.
3. H. Homma, S. Ohkita, S. Matsuda and K. Yamamoto, Weld J., 1987, **66**, 301-309.
4. K. Yamamoto et al., Proc. Symp. on Residual and Unspecified Elements in Steel, Bal Harbour Fl, 11-13 nov. 1987, ASTM, 1989, 266-284.
5. Ø. Grong, "Metallurgical Modelling of Welding-2nd Edition", The Institute of Materials, 1997.
6. B. Sundman, B. Jansson, and J.-O.Andersson, Calphad, 1985, **9**, 135-190.
7. Ø. Grong and D. K. Matlock, Int. Met. Rev., 1986, **31**, 27-48.
8. P. L. Harrison and R. A. Ferrar, Int. Mater. Rev., 1989, **34**, 35-51.
9 L. Devillers et al., Proc. Int. Conf. on Effects of Residual, Impurity and Alloying elements on Weldability and Weld properties, london, November 1983, Paper 1, Publ. The Welding Institute (England)
10. A. R. Mills, G. Thewlis and J. A. Whiteman, Mater. Sci. Technol., 1987, **3**, 1051-1062.
11. R. A. Ferrar and P. L. Harrison, J. Mat. Sci., 1987, **22**, 3812-3820.
12. "Use of Fine Inclusions in Microstructure Control of Steels, Literature Survey and Preliminary Study of Controlling Mechanism by Computer Model"; ISIJ report, 1995 (in Japanese).
13. J. Takamura and S. Mizoguchi,, Proc. of the Sixth Int. Iron and Steel Congress, Nagoya, ISIJ, 1990, p. 591-597.
14. S. Ogibayashi, K. Yamaguchi, M. Hirai, H. Goto, H. Yamaguchi, K. Tanaka, Proc. of the Sixth Int. Iron and Steel Congress, Nagoya, ISIJ, 1990, p. 612-617.
15. H. Mabuchi and T. Ohashi, "Recent progress in Structural Steel Plates as High-Tech Steels in Japan.", Berg und Hüttenmännischer Tag, Techniche Universität Bergakademie Freiberg, 20-21 June, 1996, 35-43.